JOURNAL OF AIRCRAFT
Vol. 29, No. 3, May–June 1992

Unsteady Aerodynamic Loading Produced by a Sinusoidally Oscillating Delta Wing

S. A. Huyer,* M. C. Robinson,† and M. W. Luttges‡
University of Colorado, Boulder, Colorado 80302

The unsteady aerodynamic loading produced by an oscillating delta wing was examined for a range of reduced frequencies and mean angles of attack. A three degree of freedom force balance recorded normal and tangential force data. These data were then reduced to provide unsteady lift and drag force coefficient values. The resultant aerodynamic loads were highly transient in nature and lift enhancement up to twice that of steady-state values was achieved for limiting test cases. The delta wing also experienced lift reduction during portions of the pitching cycle. Reduced dynamic drag was seen for instantaneous wing angles of attack below static stall. Hysteresis loops demonstrated the unsteadiness of the resultant flowfields and were seen for all test cases. Force balance measurements supported hypotheses on both unsteady separation mechanisms and dynamics for a delta wing. Unsteady lift integrations over time highlighted relations between reduced frequency and mean angle of attack for total bounded vorticity throughout the pitching cycle.

Nomenclature

C_d = drag coefficient
C_l = lift coefficient
C_n = normal force coefficient
C_t = tangential force coefficient
c_r = delta wing root chord
f = oscillation frequency
K = reduced frequency parameter, $\pi \times f \times c_r/V$
P = position in cycle
Re = Reynolds number, $V \times c_r/\nu$
t = time, s
t_{nd} = nondimensional time, $V \times t/c_r$
V = freestream velocity, m/s
α = wing angle of attack
α_m = mean angle of attack
ν = kinematic viscosity coefficient

Introduction

THE concept of "supermaneuverability," introduced by Herbst in the early 1980s,[1] inspired a great deal of research on poststall maneuvering through control of unsteady flowfields and thrust vectoring. Future fighter designs will rely on such techniques to extend their current performance envelopes. To exploit these flight regimes, better understanding of the unsteady and separated flows associated with pitching delta wings must be realized. Although current research that focused on pitching delta wings has documented much of the fluid phenomenology,[2–12] more research is needed to understand both these flowfields and the transient forces they produce.

Previous works have documented the vortex kinematics and resultant flowfield properties associated with pitching airfoils.[13–20] During pitch up to high angles, a dynamic stall vortex is produced. This vortex generates highly transient lift, drag, and moments on the airfoil. The peak lifting forces may be three to four times greater than maximum steady-state counterparts.

The flows produced by pitching delta wings are much more complex due to the inherent three-dimensionality of the planform. Unlike two-dimensional airfoils, a delta wing generates a conical, three-dimensional vortex structure under static conditions.[2–4] This vortex originates at the wing apex and increases in diameter along the leading edge to the trailing edge. Flow visualization by Gad-el-Hak et al.,[5] Gad-el-Hak and Ho,[6] Gad-el-Hak and Blackwelder,[7] and Gilliam et al.[8] have shown that the dominant feature of unsteady delta wing flow is also this leading-edge conical vortex. Using two-dimensional "cuts," Gilliam et al.[8] showed that this vortex resembled a dynamic stall vortex sometimes, and at other times, it resembled the conical vortex seen under static conditions. Very descriptive flow visualization photographs were presented by Freymuth.[9,10] Using three-dimensional flow visualization techniques, he showed the vortex kinematics associated with pitching delta wings. The connectivity of the vortices produced on either side of the wing was provided authenticating Helmholtz' Theorem.

Although the vortex kinematics associated with pitching delta wings has been documented relatively well, the actual unsteady aerodynamic loading produced has not. Soltani et al.[22] provided force balance data acquired from a six degree of freedom force balance for an oscillating 70 deg delta wing. They examined a range of reduced frequencies up to $K = 0.16$ for large amplitude oscillations (0–55 deg). This work provided relevant data for a limited parametric test grid. Additional data is needed to permit speculation into the physical mechanisms responsible for the observed phenomena.

This paper focused on the transient forces produced by a sinusoidally oscillating delta wing. Reduced frequency and mean angle of attack were varied for sinusoidal pitching at a fixed oscillation amplitude. Force balance data recorded effective normal, spanwise, and tangential forces produced by the resultant unsteady flowfields. These data were then normalized to provide normal, tangential, lift, and drag force coefficient data. Force coefficient data were then plotted as a function of cycle and angle of attack to demonstrate unsteady effects.

An extended parametric survey was also conducted so that differing flow mechanisms could be postulated and substantiated by the data. Force balance measurements supported

Presented as Paper 90-1536 at the AIAA 21st Fluid Dynamics, Plasma Dynamics, and Lasers Conference, Seattle, WA, June 18–20, 1990; received Aug. 6, 1990; revision received Feb. 26, 1991; accepted for publication April 5, 1991.

*Graduate Research Assistant, Department of Aerospace Engineering Sciences; currently, Post-Doctoral Research Associate, National Renewable Energy Laboratories, Golden, CO. Member AIAA.
†Assistant Professor, Department of Aerospace Engineering Sciences. Member AIAA.
‡Professor, Department of Aerospace Engineering Sciences. Member AIAA.

hypotheses on both unsteady separation mechanisms and dynamics on a delta wing. Unsteady lift integrations over time highlighted relations between K and α_m for total bounded vorticity throughout the pitching cycle.

Experimental Method

Present experiments were conducted at the University of Colorado Aerospace wind-tunnel facilities. Force balance measurements were taken in the 0.61 m × 0.61 m low-speed wind tunnel with 0.05% turbulence for a sinusoidally oscillating delta wing. The delta wing was constructed out of 1.59 mm magnesium plate. It had a 15.24 cm root chord and 45 deg sweep. Since the plate was thin, the leading and trailing edges were not beveled. Hence, the effective leading- and trailing-edge geometry was square. Static experiments conducted by Bartlett and Vidal[21] showed there was a reduction in the lift curve slope for sharp compared to rounded leading-edge geometries.

Reduced frequency K was varied by altering freestream velocity and oscillation frequency (Table 1). The maximum freestream Mach number was 0.036; hence low-speed incompressible assumptions seem appropriate. Each reduced frequency test case was examined at a mean angle of attack of 20 deg. Mean angle of attack test cases of 10, 15, 20, 25, and 30 deg were investigated at a K value of 0.2. Pitch axis location was set at the trailing edge and oscillation amplitude was held constant at 9 deg for all tests. Information regarding the effect of pitch axis location may be found in Huyer et al.[11]

The delta wing was sting mounted to the force balance at the trailing edge and was then mounted to a pitch bar. The system was driven sinusoidally by a scotch yoke mechanism powered by a 24 V dc motor with 4 to 1 gear ratio. A magnetic reed switch mounted to the flywheel of the motor, in conjunction with a period delay circuit, provided an electronic trigger pulse that was 680 μs in duration. This pulse was sampled by a Masscomp data acquisition system to insure synchronized data collection. Unless the frequency of oscillation was within 1% of prescribed values, data were not accepted. In this manner, 2 consecutive cycles were collected and averaged over 10 runs for a total of 20 cycles.

The sting-mounted force balance is shown in Fig. 1. The balance has three degrees of freedom providing normal, tangential, and spanwise force data. The normal and spanwise elements were mounted in cantilever fashion onto a steel shaft connected to the tangential element by means of a universal joint. The shaft is supported by a set of eight low-friction bearings aligned in the axial direction of the balance. The bearings were adjusted to provide an optimal balance between friction and inertial coupling. The wing was mounted directly to the force balance and was covered by a streamlined shield to guard against undesired aerodynamic loading and cooling effects. For more details concerning the force balance characteristics, the reader is referred to Huyer et al.[11]

Table 1 Experimental parameters

K	0.1	0.2	0.3	0.4	0.5
f, Hz	2.55	5.09	5.73	7.63	6.36
V, m/s	12.2	12.2	9.14	9.14	6.10
Re	102,000	102,000	76,500	76,500	51,000

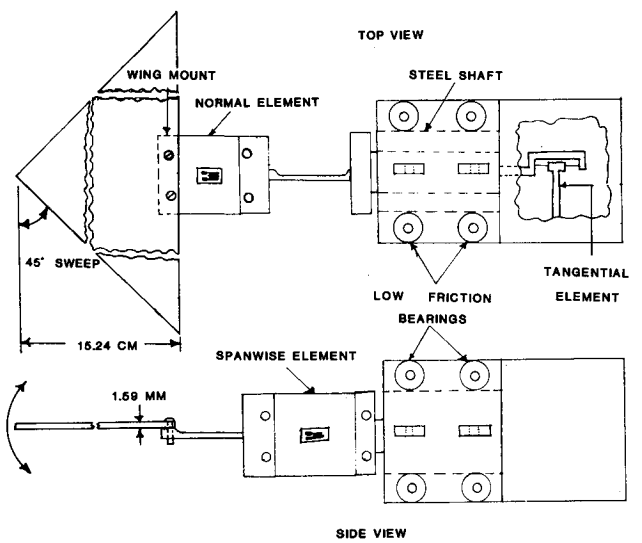

Fig. 1 Three degree of freedom sting force balance and 45 deg delta wing (not to scale); aerodynamic shield is not shown.

The ratio of the maximum area of the delta wing and force balance in the plane of the tunnel cross section to the area of the tunnel cross section was computed to establish possible tunnel blockage effects. For maximum wing incidence of 40 deg, tunnel blockage was estimated at 5.15%. Therefore, no lift correction factors for tunnel blockage were applied to static or dynamic data.

Force balance tests were conducted to examine unsteady coupling. This term refers to the spatial shift in aerodynamic center of pressure as unsteady loads are generated. The normal element was calibrated assuming the center of pressure was located at midchord in accordance with theory. Moment data were then recorded. The ratio C_m/C_n provided the approximate location of the center of pressure. Although not shown, data collected demonstrated only a modest, 5% maximum variation in center of pressure with respect to the $c/2$ point. The maximum values also occurred for minimum normal forces. It appeared that the assumption of a midchord center of pressure location was valid.

Results

To better understand the force balance data, some preliminary flow visualization tests were conducted. Flow visualization data were taken for both static and dynamic test cases. Static data revealed laminar flow conditions over the delta wing up to 2.5 deg. At α = 5 deg, initial rollup of the leading-edge vortex sheets was observed resulting in the conical vortex structures similar to that observed by Gad-el-Hak et al.[5] As α was increased to 11.25 deg, this vortex grew approximately linearly in cross-sectional area. At α = 13.75 deg, a significant increase in vortex diameter at the trailing edge was observed, possibly indicating vortex burst upstream. Similar phenomena were observed at midchord as wing incidence was increased to 16.25 deg. At α = 20 deg, the flow appeared globally separated. This means that the separated flow structures did not reattach at any point on the delta wing. Vortices produced were shed directly into the wake. Additional information on the steady and unsteady vortex kinematics is provided by Huyer and Luttges.[12]

Steady-State Results

Steady-state calibrations of the forces produced by a delta wing were performed to provide reference data for dynamic test cases. Tangential force data were found to be an order of magnitude less than normal force data. Hence, as C_l and C_d were computed, C_t values had negligible effects on C_l and had significant effects on C_d data only for angles of attack below 20 deg. Reduced C_l and C_d data are shown in Fig. 2. Data were taken from 0 to 40 deg in 2.5 deg increments to provide reference data throughout the entire dynamic angle of attack range. Data for C_l demonstrated an approximately linear increase in lift force up to α = 17.5 deg where peak lift forces were observed. As α was increased to 20 deg, only a modest decrease in C_l was observed, followed by a significant loss of lift as incidence was increased to 22.5 deg.

Data for C_d demonstrated small drag values (below 0.08) for angles of attack below 7.5 deg with a C_{d0} value of 0.04. The relatively high C_{d0} value may be attributed to the blunt leading-edge geometry. As α was increased to 10 deg, there appeared to be an increase in the drag curve slope. As α was

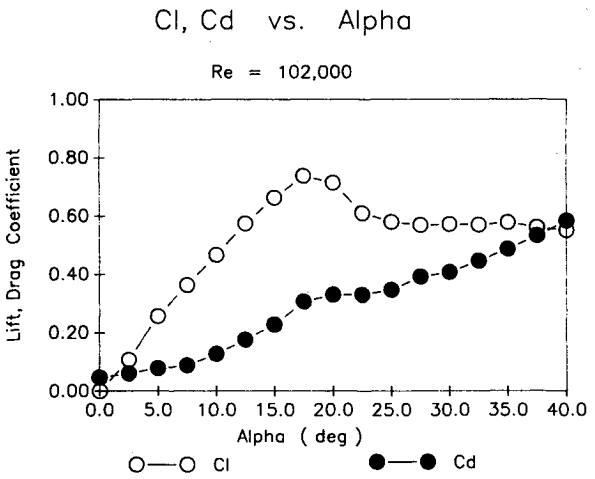

Fig. 2 Steady-state lift and drag coefficient data vs α.

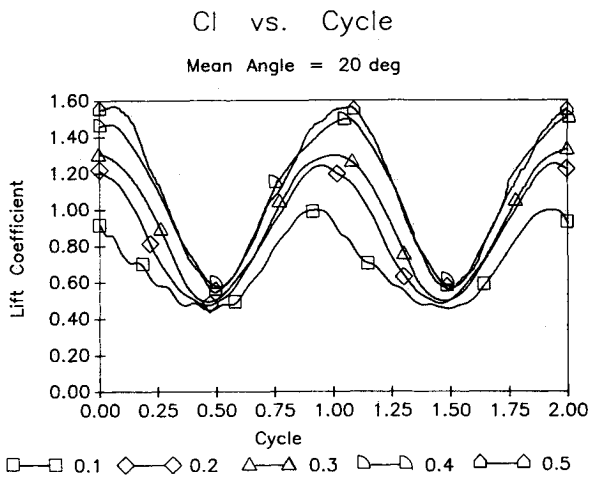

Fig. 3 Lift coefficient plotted over two consecutive cycles for α_m = 20 deg, K = 0.1, 0.2, 0.3, 0.4, and 0.5; 0.0 cycle corresponds to maximum wing angle of attack.

increased further, drag levels continued to increase sharply to C_d = 0.32 at α = 17.5 deg. As wing incidence continued to increase, drag values increased at a more moderate rate.

Effect of Reduced Frequency

Lift force coefficients are plotted as a function of cycle in Fig. 3 for reduced frequency values of 0.1, 0.2, 0.3, 0.4, and 0.5 at α_m = 20 deg. Data acquisition was initiated at maximum wing angle of attack (P = 0.0). Data for C_l appeared repeatable over the two consecutive cycles plotted. An increase in reduced frequency produced increases in maximum lift values that were delayed until later in the cycle. For K = 0.1, $C_{l\max}$ = 0.997 was observed at P = 0.92 (before maximum angle of attack). As K was increased to 0.5, $C_{l\max}$ = 1.57 was observed at P = 1.07 after the wing began to pitch down. From K = 0.01 to 0.2, $C_{l\max}$ values increased by 20%. As K was increased from 0.4 to 0.5, $C_{l\max}$ values increased by only 6%.

Similar trends were observed in Fig. 4 where C_d was plotted against cycle for selected K values. Again, the data were repeatable over two consecutive cycles. Maximum C_d values were delayed until later in the cycle, and these values increased with increased K. Values for $C_{d\max}$ ranged from 0.538 at P = 0.956 for K = 0.1 to 0.92 at P = 1.025 for K = 0.4. Values for K of 0.2, 0.3, and 0.4 demonstrated similar C_d values between P = 0.65–0.9 for positive pitch rate. Finally, $C_{d\min}$ values of approximately 0.1 were seen for all test cases at minimum incidence. Data for K = 0.5 were not presented. The low velocities required to achieve this value generated such low tangential forces that the data were deemed unreliable.

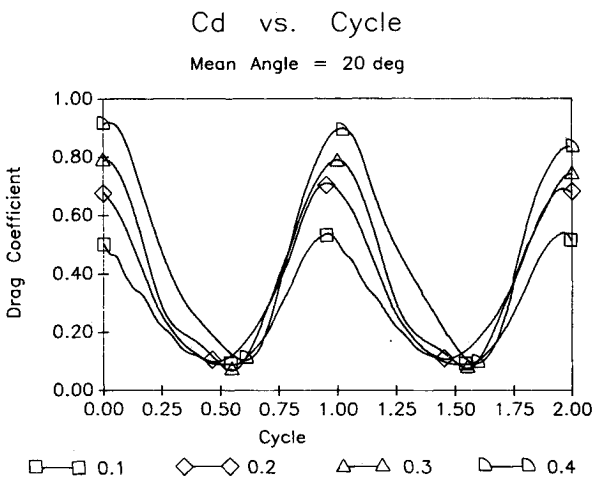

Fig. 4 Drag coefficient plotted over two consecutive cycles for α_m = 20 deg and K = 0.1, 0.2, 0.3, and 0.4.

Lift coefficient data are plotted as a function of α for K values between 0.1 and 0.5 in Fig. 5. The arrows along each trace refer to whether the wing was increasing or decreasing in incidence. The mean angle chosen produced angles of attack from 11 to 29 deg. Values for C_l at a given angle were generally different depending on positive or negative pitch rate. These hysteresis loops were formed for all K values examined. It is readily apparent that they varied in both width and character for differing reduced frequencies.

A K value of 0.1 appeared to show the widest overall hysteresis loop. Between 11 and 13 deg, this loop was narrow. As α increased, the width of this loop increased up to 20 deg where it remained approximately constant for the remaining angles. Lift reduction, compared with static values, was seen when the wing was below the static stall angle whereas lift enhancement was seen at higher angles of attack. As K was increased to 0.2, this loop became more elliptical in shape and appeared narrower compared with K = 0.1. A K value of 0.3 resulted in the formation of an even narrower hysteresis loop that became nonexistent from 28 to 29 deg. Lift enhancement was seen during positive pitch rate for these K

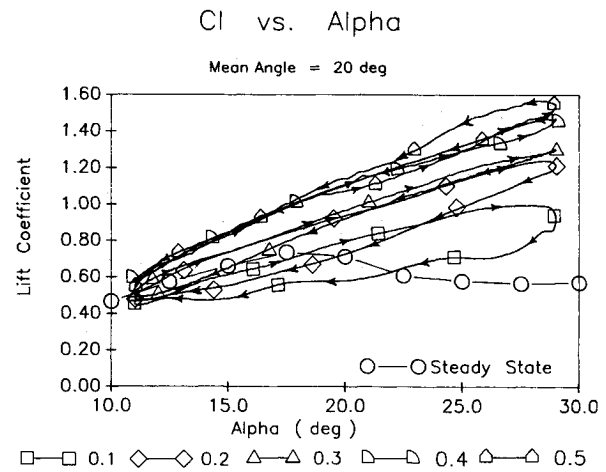

Fig. 5 Lift coefficient vs α for α_m = 20 deg and K = 0.1, 0.2, 0.3, 0.4, and 0.5. The arrows along each trace refer to wing pitch up or pitch down.

values and lift reduction was observed only below the static stall angle during negative pitching. Finally, for K = 0.1–0.3, larger C_l values were seen for increasing compared with decreasing α resulting in a clockwise loop direction.

The hysteresis loops associated with K values of 0.4 and 0.5 were different compared with the lower K values. From α = 11–19 deg, C_l values for K = 0.4 and 0.5 were identical and appeared to be independent of positive or negative pitch

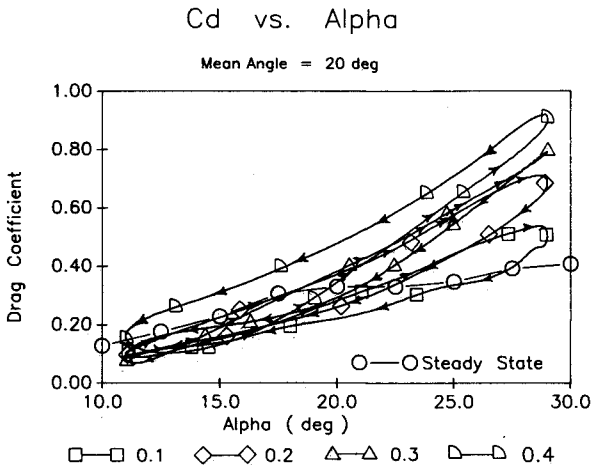

Fig. 6 Same as Fig. 5 except drag coefficient data, K = 0.1, 0.2, 0.3, and 0.4.

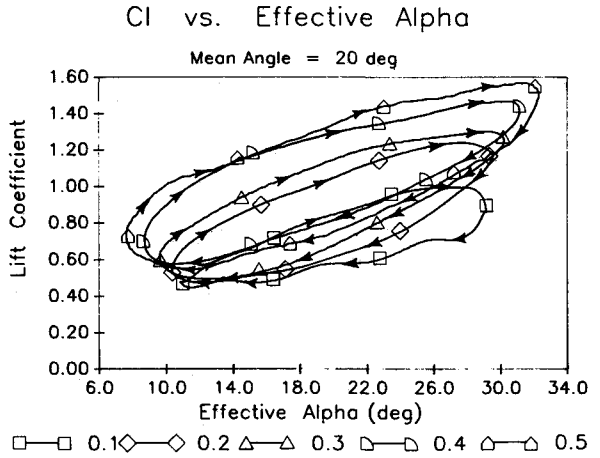

Fig. 7 Lift coefficient vs effective angle of attack for α_m = 20 deg, K = 0.1, 0.2, 0.3, 0.4, and 0.5.

rate. For K = 0.4, hysteresis was seen after 20 deg and the magnitude became larger as K was increased to 0.5. The direction of the loops were also reversed for K = 0.4 and 0.5 since peak C_l values occurred during negative pitching. Finally, lift enhancement was seen throughout the entire pitching cycle compared with static tests. For K = 0.5, C_l overshoots twice those of maximum static values were seen.

These trends were not apparent in the drag data. Figure 6 shows C_d vs α hysteresis loops for K = 0.1–0.4. For K = 0.1, the width of this loop was almost negligible between α = 11 and 14 deg at which point the loop overlaps to form a figure eight. As α was increased, the width of this loop became increasingly wider. As K was increased to 0.2, the hysteresis became greater compared to K = 0.1. The hysteresis loop associated with K = 0.3 appeared different compared with the other K values. A crossover point was observed at α = 15 deg, and the shape of the loop resembled a skewed figure eight. Also, between α = 27 and 29 deg, C_d values were identical regardless of positive or negative pitching. As K was increased to 0.4, the width of the hysteresis loop appeared greatest and the direction was reversed compared with the lower K values. Below the static stall angle, dynamic drag values were less than static counterparts except for K = 0.4 during negative pitching. A drag penalty was observed only as the static stall angle was exceeded and became more severe for increased K.

Effective angle of attack due to wing motion may have had an influence on the characteristics of the hysteresis loops associated with varying reduced frequency values. Since pitching took place at the trailing edge, the velocities at the wing apex were effectively different from those of the freestream due to the motion of the model nose relative to the freestream. The effective velocity at the wing apex was used to compute the effective angle of attack. For positive pitching, effective angle of attack was less than geometric angle of attack with the reverse being true for negative pitching.

Figure 7 shows C_l as a function of effective angle of attack for the reduced frequency test cases examined. As K was increased, the width of the hysteresis loops appeared to increase as well but only minimally. All hysteresis loops appeared elliptic in shape and differed most in terms of maximum and minimum values. Finally, the direction of the loops were clockwise for all test cases since peak C_l occurred for increasing compared to decreasing effective angles of attack.

Effect of Mean Angle

Mean angle of attack was varied to evaluate α_m effects on C_l and C_d values for angle of attack ranges from prestatic to poststatic stall. A reduced frequency value of 0.2 was used for examination of α_m = 10, 15, 20, 25, and 30 deg. For α_m = 10 deg, a 19 deg α_{max} was approximately equal to the static stall angle. For α_m = 30 deg, α_{min} = 21 deg resulted in consistent post-static stall angle of attack variations.

In Fig. 8, C_l is plotted as a function of cycle for the five mean angle of attack test cases examined. An increase in α_m resulted in earlier $C_{l\max}$ and $C_{l\min}$ values relative to cycle. Increases in α_m resulted in larger $C_{l\max}$ values but only up to α_m = 20 deg; $C_{l\max}$ = 1.24 was seen for α = 20 deg. This value was reduced to 1.23 for α_m = 25 deg and was reduced

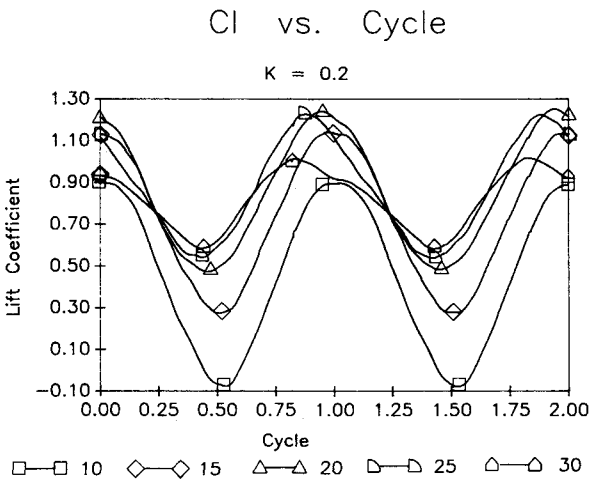

Fig. 8 Lift coefficient plotted over two consecutive cycles for K = 0.2, α_m = 10, 15, 20, 25, and 30 deg.

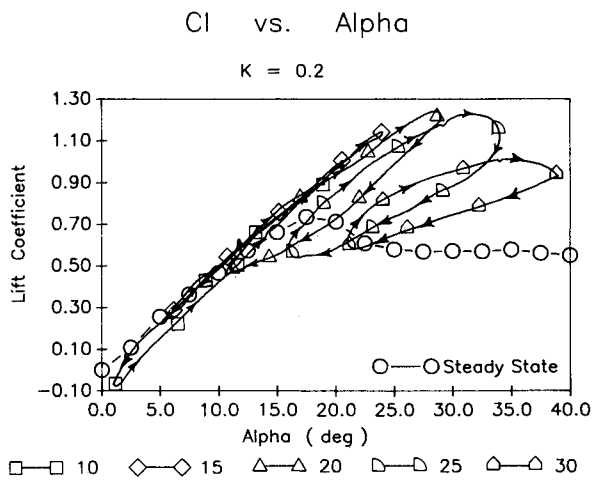

Fig. 9 Lift coefficient vs α for K = 0.2, α_m = 10, 15, 20, 25, and 30 deg.

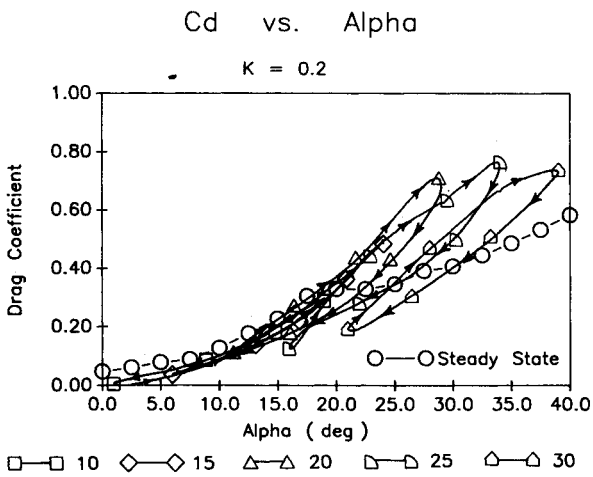

Fig. 10 Same as Fig. 9 except drag coefficient vs α.

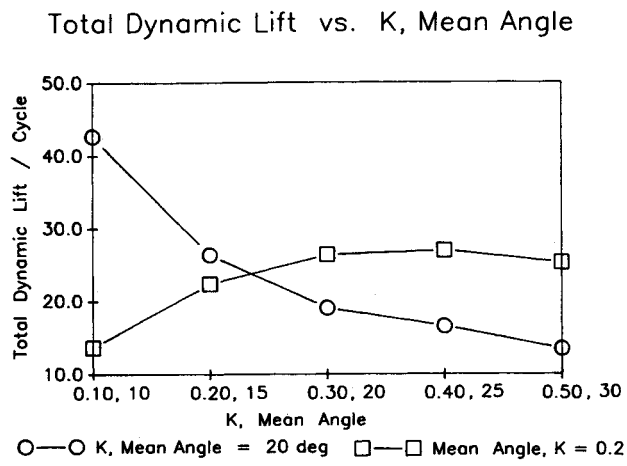

Fig. 11 Total dynamic lift/cycle as a function of K at α_m = 20 deg and as a function of α_m at K = 0.2.

significantly for α_m = 30 deg. Values for $C_{l\min}$ increased with α_m up to α_m = 30 deg. For α_m = 10 deg, negative C_l values of −0.09 were seen at P = 0.52 or in the proximity of $\alpha_{\min}$. As α_m was increased to 20 deg, $C_{l\min}$ = 0.472 was observed, and a further increase in $C_{l\min}$ to 0.583 was seen for α_m = 30 deg before $\alpha_{\min}$.

In Fig. 9, C_l was plotted as a function of angle of attack to show the hysteresis loops associated with various mean angles. Hysteresis loops associated with the two lowest mean angles (10 and 15 deg) were very narrow compared with the higher mean angles. It appeared negligible, in fact, for α_m = 15 deg. For α_m = 10 deg, this loop appeared widest at the lower angles. Hysteresis appeared negligible between 15 and 19 deg where modest lift enhancement was observed. For α_m = 10 and 15 deg, the lift curve slope followed the static data closely. As α_m was increased to 20 deg, the hysteresis loop became significantly wider and elliptical in shape. The width of the loop increased as α_m was increased to 25 deg and remained elliptical in shape. As α_m was increased to 30 deg, hysteresis and lift decreased significantly. Considerable lift enhancement was seen for higher mean angles and lift reduction observed only near minimum angles of attack. For α_m = 15 deg, consistent, although marginal, lift enhancement was observed throughout the entire pitching cycle. For all test cases, the direction of the hysteresis was clockwise except for α_m = 10 deg where the direction was reversed.

In Fig. 10, C_d is plotted as a function of α for the mean angles of attack examined. Similar trends compared to C_l data were observed. The narrowest hysteresis loop was seen for α_m = 15 deg and was slightly wider for α_m = 10 deg, especially at the lowest angles. As α_m increased to 20 deg, the width of the hysteresis became greater and appeared more elliptic in shape and somewhat skewed. As α_m was increased to 25 deg, the hysteresis loop became wider still and became slightly narrower for α_m = 30 deg. As α_m was increased, higher $C_{d\max}$ and $C_{d\min}$ values were observed. However, for all test cases, dynamic drag values were less than static counterparts for instantaneous wing angles below static stall. For α_m = 10 deg, dynamic drag values were consistently less compared with static values. Only as wing angles significantly exceeded the static stall angle were severe drag penalties observed.

Total Dynamic Lift

Although not shown, C_l was plotted as a function of nondimensional time for the reduced frequency and mean angle of attack test cases examined. As reduced frequency was increased, fluctuations in C_l occurred earlier with respect to t_{nd}. This was expected from the definition of t_{nd} and K since increased oscillation rates coupled with reduced freestream velocities would reduce the t_{nd} of the flowfield perturbations.

By integrating C_l vs t_{nd}, the area under the curve physically represented the total dynamic lift per unit cycle. This gives an indication of the total impulse imparted on the wing by the fluid. Similar methods were employed by Francis and Keesee[19] to determine optimal unsteady lift performance. Total dynamic lift was plotted as a function of both K and α_m and is shown in Fig. 11. The abscissa axis shows the K values examined at α_m = 20 deg and the α_m values examined at K = 0.2. This plot shows that an increase in K results in less total dynamic lift, and the decrease appears to drop off as $1/K$. Alternatively, an increase in mean angle results in an increase in total dynamic lift, but only up to α_m = 25 deg. As α_m was increased to 30 deg, a decrease in total dynamic lift was seen. Again, the significance of the nonlinear relationship will be demonstrated later.

Discussion

Force balance data show direct relationships between previously reported flow visualization data[2-10,12] and the transient loading experienced by an oscillating delta wing. The extensive parametric survey provided unsteady lift and drag coefficient data over a wide range of motion histories. Present tests were found to be consistent with previous two- and three-dimensional force data.[15,20,21-24] These tests allowed for hypotheses concerning unsteady and separated flow mechanisms as well as dynamics for delta wing planforms. Cyclic data demonstrated phase dependence in terms of maximum and minimum force data. Angle of attack data showed periods of lift enhancement and reduction as well as hysteresis loops. The hysteresis loops also provided evidence for differing temporal relations between unsteady and separated flow phenomena in terms of vortex initiation and global separation. Finally, the total dynamic lift described the total impulse imparted on the wing by the fluid over a single pitching cycle. As will be shown, these data permitted modest speculations about relations between K and α_m in terms of bounded vorticity present throughout the pitching cycle.

Present static C_l data were comparable with those found by Lamar[23] and Sawyer and Sullivan,[24] who used sharp leading-edge geometries (Fig. 12). Small deviations in the lift curve slope for the present experiments are consistent with those reported by Bartlett and Vidal[21] for blunt leading-edge geometries. Work by Helin[15] also demonstrated added vortex cohesiveness for sharp compared with other leading-edge geometries. It appears that sharp leading edges give rise to slightly higher circulation velocities and thus result in increased lift.

Two-dimensional tests conducted by Helin[15] and Francis and Keesee[19] showed that dynamic lift values as great as three to four times static lift values could be achieved. The effect of pitch rate or K (for the present tests) demonstrates that an increase in K results in more cohesive vortex formation and an increase in C_l overshoots.[13-20] These overshoots are

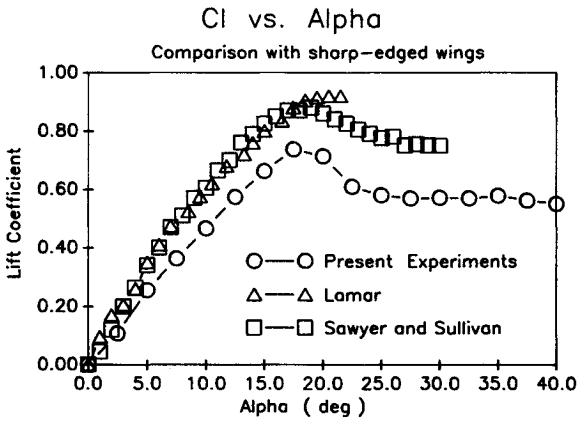

Fig. 12 Steady-state comparisons with sharp-edge 45 deg delta wings.

from dynamically exceeding maximum static lift values. For the present experiments, lift enhancement was seen for all test cases and lift reduction seen at lower K values compared to static values. Considerable C_l overshoots were seen with dynamic lift values exceeding maximum static counterparts by 100% for $K = 0.5$ and $\alpha_m = 20$ deg. Three-dimensional tests conducted by Soltani et al.[22] (delta wing) and Carta[18] (swept wing) found maximum dynamic lift values that were, at most, 25% greater than static counterparts. These tests, however, were conducted for low K values (maximum of 0.16). Considering the influence of K in terms of maximum lift overshoots and two-dimensional results, the present experiments seem consistent with the literature.[15,18,19,21]

Total dynamic lift calculations resulting from integrated C_l vs t_{nd} plots permit modest speculation about the relations between K and α_m in terms of total bound vorticity throughout the pitching cycle. The relationship between lift and circulation is well known from two-dimensional airfoil theory.[25] Spanwise integration of circulation values could provide total circulation in the case of the delta wing and can be related to lift. Additionally, the relationship between circulation and vorticity is also well known mathematically[25] and is not limited by two-dimensional constraints. Therefore, the total dynamic lift per full pitching cycle constitutes an estimate of the bounded vorticity produced on the wing over a single oscillation cycle.

As K was increased, a reduction in the total dynamic lift was seen, and this reduction appeared as approximately $1/K$. The reduction can be viewed as indicative of a reduction in bounded vorticity. As K is increased, it takes less t_{nd} to complete one oscillation cycle. Therefore, there is less fluid from which to "extract" vorticity.[16] Although less fluid is passing over the wing with time, it appears that an increase in K allows more of the vorticity that is extracted to be bound or accumulated and thus to produce enhanced lift. This idea is supported by the fact that increased K resulted in higher peak C_l values. If equal vorticity production and accumulation rates were found for each reduced frequency, a linear decrease in the total dynamic lift would have been expected.

An increase in mean angle resulted in greater total dynamic lift values, but only up to $\alpha_m = 25$ deg followed by a decrease as α_m was increased to 30 deg. These results are similar to those found by Francis and Keesee[19] who postulated an optimal maximum angle of attack in terms of lift performance for two-dimensional single pitch motions. From the theories proposed by Luttges and Kennedy,[16] an increase in mean angle results in additional amounts of vorticity production due to increased amounts of shear between the surface of a solid boundary (the delta wing) and the fluid passing over it. As α_m is increased, however, not all of the vorticity produced necessarily will be bound. Unbound vorticity does not contribute to lift. In the case of the delta wing, it is possible that some of the vorticity produced is diffused into the outer flowfield surrounding the leading-edge vortex. With increased K and α_m, the additional vorticity produced will become bound, but only up to a certain point. After certain K and α_m relations exceed a threshold, the additional vorticity produced cannot be bounded and will not produce lift.

Steady-state data showed that $C_{l\max}$ occurred at $\alpha = 17.5$ deg, but global separation did not occur until $\alpha = 20$ deg. If we extend these phenomena to dynamic test cases, force balance data provide evidence for differing temporal relations between unsteady and separated flow phenomena. The hysteresis loops highlight the persistence of circulation phenomena for these unsteady separated flow test cases. The unsteady motion histories encapsulate three major phenomena: 1) delta wing vortex initiation, 2) global separation, and 3) flow reattachment or vortex reformation. The hysteresis effects relate to temporal delays or times of occurrences related to differing wing motion histories. According to Robinson et al.,[20] wing dynamics are vital in terms of vorticity convection and accumulation time scales supporting these phenomena. The total accumulation of vorticity in an unsteady environment can be viewed as a competition between the production terms scaled by diffusion and the convective terms scaled by the freestream velocity. The wing kinematics or, in the present case, reduced frequency determine the manner in which convection and diffusion processes compete throughout the pitching cycle. For low K values, vorticity convection terms appear to be dominant whereas at high K values diffusion appears dominant. In this latter case, increased vorticity accumulations occur.

The hysteresis loops were present for lower K values (0.1–0.3). At the higher angles for K values of 0.4 and 0.5, the hysteresis effects were reversed in direction. The reversals were related to the $C_{l\max}$ being attained only after $\alpha_{\max}$ had been reached. At lower K values, the flow appears to become globally separated before $\alpha_{\max}$. In these cases, a decrease in lift occurred as the wing continued to pitch up. Such observations suggest that for low K values, vorticity convection terms dominate. Since the flow would hypothetically lack vorticity, circulation velocities would be minimal, resulting in loss of lift. As the wing pitched down, hysteresis fluid effects result in delayed flow reattachment, and reduced lift values occur.

For $K = 0.3$, $C_{l\max}$ occurred at $\alpha_{\max}$. From static results, the wing should not yet show global separation. Thus, the reductions in lift remain to be explained. As the wing pitched down, higher effective angles of attack were attained that would support a globally separated flowfield. Also, when $C_{l\max}$ is reached, any pitch down coupled with hysteresis should be sufficient to cause global separation. In other words, there would be no way to prevent the phenomenon.

As K was increased to 0.4 and 0.5, the lift data strongly supported the notion that globally separated flow conditions over the delta wing did not occur even at maximum angles of attack. Lift enhancement was seen throughout the entire oscillation cycle. The increased circulation velocities associated with the leading-edge vortex structures undoubtedly were large, and presumably the dominance of vorticity diffusion terms resulted in increased vorticity accumulations. The magnitude of lift enhancement produced as K was increased from 0.4 to 0.5 was smaller compared with K increases from 0.1 to 0.2. This may indicate a point of diminishing returns for lift enhancement. Even though the flowfield would not be globally separated, in terms of bounded vorticity, further increases in K should lead to less vorticity production and to lower circulation velocities even though relative vorticity accumulation is increased. The present experiments could not confirm this limit since $K = 0.5$ was the maximum value possible for the present experimental configuration. Experiments conducted by Francis and Keesee[19] support the possibility of a ceiling on lift enhancements.

For $\alpha_m = 10$ deg, negative lift values were observed proximal to minimum α (1 deg). Flow visualization data revealed a chaotic flowfield over the wing upper surface at 1 deg and laminar flow at 3.5 deg. It is likely that the shedding of the

leading-edge vortex resulted in destructive flow interactions with either the surface or outer flowfield or both. The chaotic flowfield over the upper surface presumably would produce higher pressures over the upper surface with respect to the lower surface, accounting for negative C_l values. This too would account for the hysteresis seen in the lift data. Lift reduction could be attributed to delayed vortex initiation to higher angles of attack relative to static values.

As α_m was increased to 15 deg, the lift curve slope followed the static lift curve slope almost exactly and a linear increase in lift was seen from 6 to 24 deg. Also, the width of the hysteresis loop was negligible. Separated flow mechanisms seen here may be similar to those seen for the high K values at α_m = 20 deg. Force balance data suggest that global separation was eliminated, allowing for bounded vortex structures throughout the entire cycle.

The higher mean angles examined (20, 25, and 30 deg) resulted in a consistent increase in the width of the hysteresis loops. This occurred since $C_{l\max}$ was attained before $\alpha_{\max}$. It is likely that global separation occurred before reaching $\alpha_{\max}$ and occurred earlier in the cycle as α_m was increased. At α_m = 20 deg, however, peak C_l values were observed. It is likely that additional vorticity production resulted in increased circulation velocities, accounting for the lift enhancement. Significant lift enhancement was observed at α_m = 30 deg even though the wing performed consistent post-stall maneuvers.

A factor influencing global separation is the persistence of the adverse pressure gradient. Adverse pressure gradients are known to greatly influence flow separation in two-dimensional static flowfields.[25] Static tests conducted by Roos and Kegelman[26] on a delta wing showed greater leading-edge suction pressure peaks as incidence was increased. These peaks indicate the presence of strong adverse pressure gradients inboard. Extending these results to dynamic test cases, an increase in α_m likely produced stronger adverse pressure gradients. Cyclic data showed that as α_m was increased, maximum lift values occurred earlier in the cycle. This demonstrates the increased strength of the adverse pressure gradient as α_m was increased. Dynamic pitching, however, resulted in delaying the effects of the adverse pressure gradient.

The delta wing planform exacts special constraints on the way unsteady separated flows can interact. For a three-dimensional wing, there is a leading edge, a trailing edge, and two wing tips. The resultant dynamic stall vortex may interact with the wing tip vortices. This is not the case for a delta wing. Here, leading edge and wing tips are merged. Under static conditions, these conical vortices are analogous to wing tip vortices, although there are important differences. This special geometry limits the type of unsteady flowfields that can be produced. Only leading-edge vortex structures are produced. Also, there are limits in the way these vortices can interact with the surface. Interactions occur inboard and downstream from the leading edge. In addition, three-dimensional convection properties are likely.

Conclusions

Complex lift enhancement and reduction histories were seen for differing pitching delta wing tests. Dynamic lift values twice those of static counterparts were observed. In addition, drag reduction was seen for all dynamic test cases having angles of attack below the static stall angle. Drag penalties, likely due to the lift enhancement achieved, were seen only at angles of attack exceeding static stall.

Hysteresis loops were seen in all test cases but exhibited differing characteristics depending on motion history. For low mean angles, hysteresis was observed and was found to be counterclockwise in direction. Moderate reduced frequencies coupled with low mean angles showed little hysteresis. As mean angle was increased, however, hysteresis became greater and was clockwise in direction. As reduced frequency was increased, hysteresis was seen only at higher angles of attack and the loops were counterclockwise in direction.

The hysteresis loops highlight the persistence of circulation phenomena for these unsteady separated flow test cases. They also relate to temporal delays or times of occurrences associated with differing wing motion histories. It was postulated that high K values or low mean angles eliminated the onset of global separation. Low K or higher mean angle of attack test cases produced global separation before maximum angle of attack. The former tests yield lift enhancement, but the latter demonstrated periods of lift deterioration.

Total dynamic lift calculations permitted modest speculation about the relations between reduced frequency and mean angle of attack in terms of bounded vorticity throughout the pitching cycle. As K was increased, a reduction in total dynamic lift as $1/K$ was seen. The reduction could be viewed as indicative of a reduction in bounded vorticity. An increase in mean angle resulted in greater total dynamic lift values, but only up to α_m = 25 deg. It was postulated that with increased K, additional vorticity produced will become bound, but only up to a certain point. After K and α_m relations exceed a threshold, the additional vorticity produced cannot be bounded and will not produce lift.

It is clear that the unsteady flows produced by an oscillating delta wing produced substantial effects in terms of aerodynamic loading. Future work should concentrate on specific vortex kinematics and hysteresis effects generated across a wider range of motion histories. These and the present studies will provide the information and understanding fundamental to the potential exploitation and application of these unsteady flowfields.

Acknowledgments

This work was sponsored, in part, by the USAF Office of Scientific Research, Grant F49620-84-C-0065, James McMichael and Hank Helin, program managers. The authors greatly appreciated the technical assistance of W. Bank as well as of R. Meinzer, whose assistance in the design and construction of the force balance used in the present experiments proved invaluable.

References

[1]Herbst, W. B., "Supermaneuverability," *Workshop on Unsteady Separated Flows*, U.S. Air Force Academy, Colorado Springs, CO, Aug. 1983, pp. 1–9.

[2]Lee, G. H., "Note on the Flow Around Delta Wings with Sharp Leading Edges," Aeronautical Research Council, R&M 3070, Sept. 1955.

[3]Lambourne, N. C., and Bryer, D. W., "The Bursting of Leading Edge Vortices; Some Observations and Discussion of the Phenomenon," Aeronautical Research Council, R&M 3282, April 1961.

[4]Lee, M., and Ho, C. M., "Vortex Dynamics of Delta Wings," *Applied Mechanics Review*, Vol. 43, Sept. 1990, pp. 365–427.

[5]Gad-el-Hak, M., Ho, C. M., and Blackwelder, R. F., "A Visual Study of a Delta Wing in Steady and Unsteady Motion," *Workshop on Unsteady Separated Flows*, U.S. Air Force Academy, Colorado Springs, CO, Aug. 1983, pp. 45–51.

[6]Gad-el-Hak, M., and Ho, C. M., "The Pitching Delta Wing," *AIAA Journal*, Vol. 23, No. 11, 1985, pp. 1660–1665.

[7]Gad-el-Hak, M., and Blackwelder, R. F., "Control of the Discrete Vortices from a Delta Wing," *AIAA Journal*, Vol. 25, No. 8, 1987, pp. 1042–1049.

[8]Gilliam, F., Wissler, J., Robinson, M., and Walker, J., "Visualization of Unsteady Separated Flow about a Pitching Delta Wing," AIAA Paper 97-0240, Jan. 1987.

[9]Freymuth, P., "Progress in Visualizing Unsteady Separation," *Workshop II on Unsteady Separated Flows*, U.S. Air Force Academy, Colorado Springs, CO, July 1987, pp. 197–210.

[10]Freymuth, P., "Visualizing the Connectivity of Vortex Systems for Pitching Wings," 1st National Congress of Fluid Mechanics paper AIAA-88-3549-CP, Cincinnati, OH, July 1988.

[11]Huyer, S., Robinson, M., and Luttges, M., "Unsteady Aerodynamic Loading Produced by a Sinusoidally Oscillating Delta Wing," AIAA Paper 90-1536, June 1990.

[12]Huyer, S., and Luttges, M., "The Vortex Kinematics Associated

with an Oscillating Delta Wing," AIAA Paper 91-1797, June 1991.

[13]Huyer, S., Reavis, M., and Luttges, M., "A Comparative Study of Differing Vortex Structures Arising in Unsteady Separated Flow," AIAA Paper 88-2582, June 1988.

[14]Walker, J. M., Helin, H. E., and Strickland, J. H., "An Experimental Investigation of an Airfoil Undergoing Large Amplitude Pitching Motions," *AIAA Journal*, Vol. 23, No. 8, 1985, pp. 1141–1142.

[15]Helin, H., "Experimental Studies on the Dynamic Development and Control of Unsteady Separated Flows," Doctoral Thesis, Department of Aerospace Engineering Sciences, Univ. of Colorado, Boulder, CO, 1986.

[16]Luttges, M., and Kennedy, D., "Initiation and Use of Three-Dimensional Unsteady Separated Flows," *Workshop II on Unsteady Separated Flows*, U.S. Air Force Academy, Colorado Springs, CO, July 1987, pp. 211–224.

[17]Reynolds, W. C., and Carr, L. W., "Review of Unsteady, Driven, Separated Flows," AIAA Paper 85-0527, March 1985.

[18]Carta, F. O., "Unsteady Stall Penetration of an Oscillating Swept Wing," *Workshop on Unsteady Separated Flows*, U.S. Air Force Academy, Colorado Springs, CO, Aug. 1983, pp. 28–37.

[19]Francis, M. S., and Keesee, J. E., "Airfoil dynamic Stall Performance with Large-Amplitude Motions," *AIAA Journal*, Vol. 23, No. 11, 1985, pp. 1653–1659.

[20]Robinson, M., Walker, J., and Wissler, J., "Unsteady Surface Pressure Measurements on a Pitching Rectangular Wing," *Workshop II on Unsteady Separated Flows*, U.S. Air Force Academy, Colorado Springs, CO, July 1987, pp. 225–237.

[21]Bartlett, G. E., and Vidal, R. J., "Experimental Investigation of Influence of Edge Shape on the Aerodynamic Characteristics of Low Aspect Ratio Wings at Low Speeds," *Journal of Aerospace Science*, Vol. 22, Aug. 1955, pp. 517–533.

[22]Soltani, M., Bragg, M., and Brandon, J., "Experimental Measurements on an Oscillating 70° Delta Wing in Subsonic Flow," AIAA Paper 88-2576, June 1988.

[23]Lamar, J. E., "Recent Studies of Subsonic Vortex Lift Including Parameters Affecting Stable Leading-Edge Vortex Flow," *Journal of Aircraft*, Vol. 14, No. 12, 1977, pp. 1205–1211.

[24]Sawyer, R., and Sullivan, J., "Lift Development of Delta Wings Undergoing Constant Acceleration from Rest," AIAA Paper 90-0310, Jan. 1990.

[25]Thwaites, B., *Incompressible Aerodynamics*, 1st ed., Dover, New York, 1960, pp. 32–33, 191–194.

[26]Roos, F. W., and Kegelman, J. T., "An Experimental Investigation of Sweep-Angle Influence on Delta-Wing Flows," AIAA Paper 90-0383, Jan. 1990.